Chapter 18
Electromagnetic Modes Inside the Island Kind 2D Photonic Crystal Resonator

E. Ya. Glushko and A. N. Stepanyuk

18.1 Introduction

The existing terminology distinguishes several kinds of photonic structures: photonic crystals, photonic membranes and photonic crystal resonators. An infinite 2D structure periodically ordered in *ZY* plane and having also infinite size in *Z* direction is called a photonic crystal whereas the photonic crystal resonator has finite sizes in *ZY* plane and perfectly smooth boundaries with external medium. This circumstance generates a clear expressed angular area of total internal reflection of field inside the resonator for in-plane geometry. In general case, a resonator has infinite size in *X* direction. The only way to excite a standing wave inside exists through the input prisms due to that the external beam may hit into the total internal reflection area of the resonator. The photonic membrane may be treated as a thin photonic crystal dividing the external medium into two parts and transmitting radiation from one medium to another [1]. At the present time the photonic crystals (PhC) have been widely investigated as perspective objects of optical technologies in computing, signal processing, telecommunication, sensoring, etc. [2, 3] though in the main, the 2D PhC is considering only as a perfect reflecting medium surrounding an optical waveguide. Therefore the conditions of omnidirectional gaps in photonic spectrum are of interest for the determination of the optimal wavelength range of optical devices [4–7]. Meanwhile optical properties of photonic crystals may be

E.Y. Glushko (✉)
Institute of Semiconductor Physics, National Academy of Sciences of Ukraine, 41 Nauki Prsp, Kyiv 03028, Ukraine
e-mail: scientist.com_eugene.glushko@mail.com

A.N. Stepanyuk
Kryvyi Rih State Pedagogical University, Gagarin pr., 54, 50086 Kryvyi Rih, Ukraine

O. Fesenko, L. Yatsenko (eds.), *Nanophysics, Nanomaterials, Interface Studies, and Applications*, Springer Proceedings in Physics 195,
DOI 10.1007/978-3-319-56422-7_18

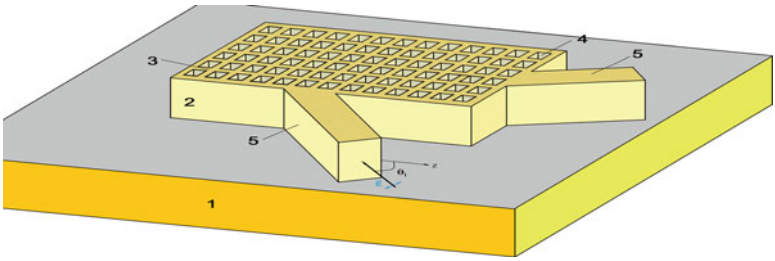

Fig. 18.1 Sketch of the island type binary 13 × 6 period 2D photonic crystal resonator (ICPR). *1* substrate, *2* covering layer, *3* matrix material, *4* accompanying material (shown air wells), *5* input-output waveguides, θ_1, angle of incidence, *p*-polarized plane wave

important for a wide area of applications in optoelectronic and all-optical devices. Further development of this area may be related to more detailed consideration of the influence of a resonator's finite sizes on the modal structure and features of field modal distribution inside a finite photonic crystal. A number of FDTD investigations exist devoted to wave transmission through the infinite 2D PhCr of various symmetries (see review [8]) whereas resonators of finite sizes need a more adequate mathematical model. The proposed island 2D resonator is a generalized kind of the 2D photonic crystal, (Nz, $N_Y \rightarrow \infty$) which, the resonator, has finite sizes in two directions and perfect external faces (Fig. 18.1). In [8, 9] the properties of finite resonators were estimated in the framework of perturbation theory. It was found there that small parameter exists for the problem of captured within the total internal reflection (TIR) domain electromagnetic field in a finite dielectric structure with spatially piecewise alternating index of refraction. The condition of small parameter existence is based on demand electromagnetic energy inside the resonator which is much more than energy of the mode tails outside the resonator. Therefore, the number of periods in both directions should be more than 10–12. The small parameter existence and an appropriate realization of the perturbation theory were demonstrated in [9, 10] for the case of weak intrinsic optical contrast of the dielectric photonic structure (see [11]).

In Fig. 18.1, a binary island kind $N_z \times N_y$ period photonic crystal resonator (IPCR) grown on a substrate 1 and consisting of matrix material 3 with refractive indices n_1 pierced with a regular system of wells/bars 4 having refractive indices n_2. If the external covering layer 2 consists of the optically nonlinear material, an opportunity arises to control the beam entrance angle into the resonator. It is worth noting that matrix material is topologically connected whereas the embedded into the matrix ordered bars or wells of a concomitant material are disconnected. This circumstance is important for the method to calculate field in a finite resonator developed below.

The resonator in-plane standing modes can be excited by an external source through the special inputs 5 and may be controlled due to their nonlinear properties. The photonic modes differ in terms of field density distribution inside the resonator,

their dependence on frequency and geometry of incidence that may be used in optical devices to control light energy flows and perform logic operations.

In this work, a binary island kind photonic crystal resonator is investigated analytically and numerically in the framework of standing wave expansion (SWE) method. We have calculated parametric dependencies of modes energy for silicon glass resonator and considered a way to classify the resonator's eigenstates. The field distribution inside the resonator is calculated at different parameters, and ways of use the switching states in optical devices are discussed.

18.2 SWE Theory for Electromagnetic Field in a Finite 2D Photonic Crystal

The standing wave expansion (SWE) approach is based on the representation of a 2D eigenstate of a resonator as the expansion in eigenstates produced by two crossed in Z and Y directions and superposed finite binary 1D photonic crystals. The eigenvalue problem is analytically solved separately for two probe 1D PhCrs and resulting 2D basis is generated as a direct production of separated 1D bases $\{|s>_z\}$ and $\{|g>_y\}$ [6], where $s, g = 1, 2, \ldots m$, correspondingly the 2D basis size is m^2. Due to the rectangular form of the resonator, the incident angles of waves united in a 2D basis function $|\, s(\theta_1)\, g\left(\theta_1^{'}\right) >$ are correlated $\theta_1 = \pi/2 - \theta_1^{'}$, where the subscript (') refers to the optically more dense matrix medium, θ_1 is the wave angle of incidence relatively Z-axis in matrix material. Suppose the materials constituting the photonic crystal are optically linear, isotropic and nonmagnetic and free charges are absent, the following equation for electromagnetic field in a continuous medium with piecewise constant refractive index

$$\frac{1}{\varepsilon(z, y)} \Delta \vec{E} + \frac{\omega^2}{c_2} \vec{E} = 0 \tag{18.1}$$

can be expanded into the 2D basis $|\, s(\theta_1)\, g\left(\theta_1^{'}\right) >$ series. The piecewise constant dielectric function $\varepsilon(z, y)$ is factored out through the Laplace operator, therefore solutions of both probe 1D problems are the plane wave based standing modes. In the considered case of p-polarization, a convenient basis of functions $M^{sg}(z, y)$ may be built in several ways: on the magnetic field components, on tangential components of electric field and on normal components of the electrical induction. A set of eigenfunctions based on magnetic field was investigated in [8, 9]. Here we consider the normal components of electrical induction as the modes $M^{sg}(z, y)$ of initial basis, where $s = 1.s_{\max}$, $g = 1.g_{\max}$. The physical restrictions demand the mode to be a continuous function of variables z and y but the derivatives may have a jump because the standing waves do not convey energy. Below, we study the rectangular photonic crystal resonator based on a 2D terminated binary

structure consisting of the topologically connected matrix material and another one – disconnected material 4 (Fig. 18.1), which looks like a system of rectangular bars. Therefore the resonator may be divided into *ij* areas by the number of periods N_z, N_y in Z and Y directions, where $i = 0,1... 2N_z + 2$, $j = 0,1... 2N_y + 2$. The outside areas are described by indices $i = 0, 2N_z + 2$, $j = 0, 2N_y + 2$ and the solution of (18.1) contains here at least one exponentially decreasing with distance factor. Inside the IPCR body, the indices i, j run from 1 to $N_z + 1$ or $N_y + 1$. Then a mode in an intrinsic area *ij* may be presented in a view:

$$M_{ij}^{sg}(z,y) = A_{zi} \bullet \sin\theta_i \bullet \varepsilon_i \bullet \cos\left(k_{is} z + \psi_{is}\right) \bullet A_{yj} \sin\theta_j \bullet \varepsilon_j \bullet \cos\left(k_{jg} y + \psi_{jg}\right), \tag{18.2}$$

where $\varepsilon_{i,j}$ denotes dielectric function in matter of the resonator area i or j. The amplitudes A_{zi}, A_{yj} and phases ψ_{is}, ψ_{jg} are analytically obtained in the framework of the 1D problem for two probe crossed photonic crystals inside intrinsic areas $j,i = 1,2... 2N + 1$, whereas for outside areas where $i = 0$ or $j = 0$ the cosines should be replaced by $\exp(-k_{is}z)$ or $\exp(-k_{jg}y)$, correspondingly. The wave front orientation with respect to OX axes is given by angle $\theta_i = \theta_1$ or θ_2 for odd or even layers of a probe 1D PhCr with the same materials and appropriate geometry [8]. The angles θ_j presented in Y-part of the basis function are $\pi/2-\theta_1$ and $\pi/2-\theta_2$ for odd or even layers, respectively. Here, the index 1 corresponds to matrix material and index 2 denotes the embedded into the matrix ordered bars of another material. The indices s, g enumerate eigenstates of two probe 1D problems solved for Z degrees of freedom at the incident angle θ_1 and for Y direction at the incident angle θ_1'.

$$\begin{aligned} \overrightarrow{E_i} &= (\sin\theta_i, \cos\theta_i) A_{zi} e^{ik_{iz}z} + \\ &(\sin\theta_i, -\cos\theta_i) B_{zi} e^{-ik_{iz}z} \\ \overrightarrow{E_j} &= \left(\sin\theta_j', \cos\theta_j'\right) A_{yj} e^{ik_{jy}y} + \\ &\left(\sin\theta_j', -\cos\theta_j'\right) B_{yj} e^{-ik_{jy}y} \end{aligned} \tag{18.3}$$

The amplitudes A, B ($A^* = B$ in the considered case) are found in the framework of both probe problems from the system of boundary conditions taken at $2N_{z(y)} + 1$ alternating boundaries [8–10]. Further, the boundary conditions of continuity for the normal component of electrical induction (mode) at both surfaces of each layer of the probe 1D PhCr lead to the system of equations for unknown amplitudes. In matrix view we have the system of equations

$$\begin{cases} \widehat{R}_l \begin{pmatrix} A_l \\ B_l \end{pmatrix} = \widehat{L}_1 \begin{pmatrix} A_1 \\ B_1 \end{pmatrix} = \\ \widehat{R}_1^{-1} \bullet \widehat{L}_2 \begin{pmatrix} A_2 \\ B_2 \end{pmatrix} = \\ \widehat{R}_2^{-1} \bullet \widehat{L}_3 \begin{pmatrix} A_3 \\ B_3 \end{pmatrix} = \ldots \\ = \widehat{R}_{2N}^{-1} \bullet \widehat{L}_{2N+1} \begin{pmatrix} A_{2N+1} \\ B_{2N+1} \end{pmatrix} = \\ A_r \widehat{R}_{2N+1}^{-1} \bullet \widehat{L}_r \begin{pmatrix} \cos\theta_r \\ \varepsilon_r \sin\theta_r \end{pmatrix} \end{cases}, \tag{18.4}$$

where $\widehat{L}, \widehat{\mathrm{R}}$ are binary matrices of boundary conditions of probe problem for a layered photonic crystal, indices 1 ($i,j = 0$) and r ($i,j = 2N_{z(y)} + 2$) describe the external medium and topology demands $\varepsilon_1 = \varepsilon_r$. The set of 1D functions $\{|s>_z\}$ and $\{|g>_y\}$ should possess the properties of a basis: completeness, orthogonality, right position and number of nodal points. Nevertheless, we observed the affinity of the calculated basis expressed in a weak (5%) non-orthogonality between states of the same parity. We suppose that the 1D basis affinity is caused by dielectric function jumps at the layer boundaries. Further, using the Gram-Schmidt procedure of orthogonalization separately for odd and even subgroups of states, the basis is transformed to the needed orthogonal form.

The expansion of a mode σ into the series gives

$$M_\sigma(z,y) = \sum_{s,g} h_{sg}^\sigma \cdot |\, s,g > \tag{18.5}$$

Then, Eq. (18.1) generates the system of equations for expansion amplitudes h_{sg}:

$$\begin{cases} \sum\limits_{s,g} \left[< q| \frac{k_{sg}^2}{\varepsilon(x,y)} |sg> - \frac{\Omega^2}{c^2} \delta_{q,sg} \right] h_{sg} \\ q = 1..N_m \end{cases}, \tag{18.6}$$

where q numbers state the 2D basis, $N_\mathrm{m} = s_\mathrm{max} \cdot g_\mathrm{max}$; matrix element $<q|\mathrm{k}^2{}_{sg}/\varepsilon(x, y)|s, g>$ means the integral is over the resonator and surrounding medium; wave vector k_{sg} is also a piecewise continuous constant. It should be noted that matrix elements have the analytical form in our approach because the modes M presented in formula (18.2) are described by amplitudes $A_{zi}(s)$, $A_{yj}(g)$ and phases ψ_{is}, ψ_{is} found in two 1D problems for crossed layered structures [8]. These two problems play the part of a 2D basis generator. The full solution of the IPCR system is given by a multitude of eigenvalues $\Omega_\mathrm{q}{}^2$ and corresponding standing waves, resonator modes.

$$\left\{ \Omega_\sigma^2 , \begin{pmatrix} h_1^\sigma \\ \ldots \\ h_{N_m}^\sigma \end{pmatrix} \right\}, \tag{18.7}$$

where σ enumerates standing waves inside the total internal reflection area of the resonator and $h^{\sigma}{}_{m}$ are coefficients of the 2D state σ expansion into initial basis $|s, g>$ series.

The developed approach differs from the calculation methods for infinite structures like the plane wave expansion method (PWEM) due to the essential non-periodicity of integrals $<q|k^2{}_{sg}/\varepsilon(x, y)|s, g>$ in (18.6) that leads to additional $4(N_z + 1)(N_y + 1)$ separate integrals for the total number of ij areas. As a result, the modes q described by expansion coefficients $h^{q}{}_{sg}$ are far from periodicity along the IPCR body. As an advantage of this method, one can note that the number of states $|s, g>$ taken to form the 2D basis may be essentially less than in the case of PWEM due to their initial nearness to needed solutions. Especially when it concerns the local states and low-energetic modes with small number of knot lines. Besides, the multitude of states $|s, g>$ can be formed in accordance with the energy interval under consideration.

To analyse eigenstates inside the IPCR, we have calculated the 19 × 19-period (SiO_2/SiO_2) 2D IPCR consisting of rectangular glass wells with sides $b_z = 1.0$ μm, $b_y = 1.1$ μm and $\varepsilon_2 = 2.25$ periodically distributed in the optically more dense glass matrix with dielectric function $\varepsilon_1 = 3.61$. The optically lesser contrast IPCR (Fig. 18.2a–c) has the period along Z axis $d_{z.} = a_z + b_z = 3.0$ μm as well as along Y axis $d_y = a_y + b_y = 3.0$ μm. The total sizes of the IPCR in this case are 59 × 58.9 μ including the covering layer. The optically bigger contrast IPCR (Fig. 18.2d)

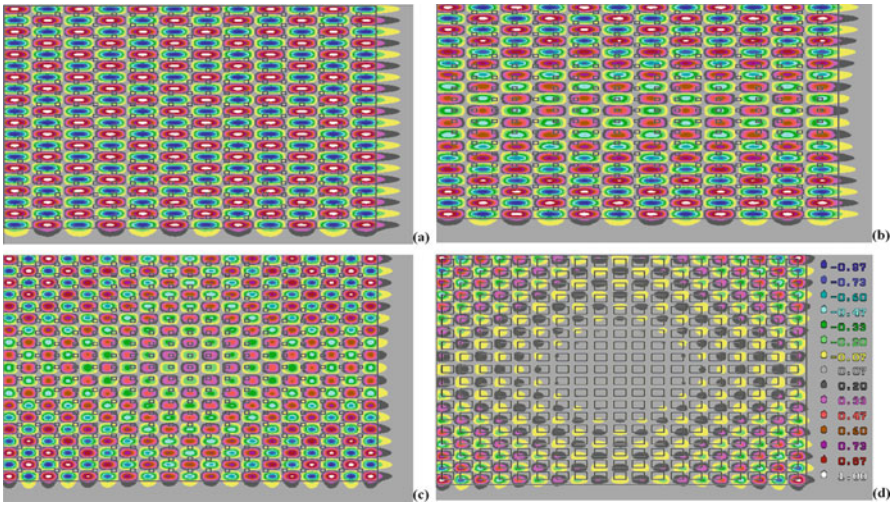

Fig. 18.2 Photonic mode distribution patterns for the 19 × 19 period 2D IPCR (*left* and *upper* external parts are cut). SiO_2/SiO_2 structure $b_z = 0.5$ μm, $b_y = 0.6$ μm, $d_{z.} = 2.0$ μm, $d_y = 1.8$ μm. Modal Msg distribution (**a**) band mode $s = 12$, $g = 20$, $\theta_1 = \pi/4$; (**b**) local surface mode $s = 12$, $g = 19$, $\theta_1 = \pi/4$; (**c**) local edge mode, $s = 19$, $g = 19$, $\theta_1 = \pi/4$ (lower contrast); (**d**) local edge mode, $s = 19$, $g = 19$, $\theta_1 = \pi/4$ (higher contrast, $b_z = 1.0$ μm, $b_y = 1.1$ μm, $d_{z.} = 3.0$ μm, $d_y = 3.0$ μm)

has the period along Z axis $d_z = a_z + b_z = 2.0$ μm as well as along Y axis $d_y = a_y + b_y = 1.8$ μm, then we have total sizes of the IPCR 39.5×35.4 μ including the covering layer. The difference in optical contrasts for structures based on the same materials is explained by wider gaps for this geometry [10]. In Fig. 18.2a, shown is a typical band mode, energy $\Omega_{sg} = 0.333$ eV, $s = 12$, $g = 20$, uniformly distributed inside the resonator's body. The part of field energy outside the IPCR in mode M_{sg} tails is small in comparison with the bulk part. This circumstance is the reason of small parameter existence and serves as a base of perturbation theory for field in a resonator of finite sizes [11]. In Fig. 18.2b, field amplitude distribution is shown for the local surface mode $s = 12$, $g = 19$ with energy $\Omega_{sg} = 0.327$ eV which is characterized by dominating density of electromagnetic energy near both resonator surfaces parallel to OZ axis (Fig. 18.1). The case of edge local modes is presented in Fig. 18.2c (lower contrast, $s = 19$, $g = 19$, $\Omega_{sg} = 0.378$ eV) and Fig. 18.2d (higher contrast, $s = 19$, $g = 19$, $\Omega_{sg} = 0.306$ eV). Depending on the intrinsic optical contrast, the edge-kind local mode concentrates its density mainly near the edges inside the IPCR.

18.3 Mode Energy Angular Diagram for an Island Resonator

The island kind photonic resonator being principally a finite size object serving to concentrate the electromagnetic energy inside should be described by a basis set of 2D eigenfunctions which have finite amplitudes in the resonator's volume with decreasing to zero outside the IPCR. The electromagnetic flow of resonance frequency passes into the IPCR through the input and go out through the output prism (Fig. 18.1). The gain may be reached due to an appropriate ratio of input-output sections. One more circumstance is that the IPCR is a convenient system to operate the separate modes due to distinctive difference in their energies and wave vectors.

We have calculated the 6×7-period (SiO_2/SiO_2) 2D IPCR consisting of rectangular glass wells with sides $b_z = 1.0$ μm, $b_y = 2.0$ μm and $\varepsilon_2 = 2.25$ periodically distributed in the optically more dense glass matrix with dielectric function $\varepsilon_1 = 3.24$ so that the period along Z axis is $d_z = a_z + b_z = 2.5$ μm and along Y axis is $d_y = a_y + b_y = 3.0$ μm. The total sizes of the IPCR are 16×22 microns including the covering layer.

The multitude of modes having the given number of nodal lines forms a branch in the TIR domain (Θ_{TIR}, $\pi/2$-Θ_{TIR}). In Fig. 18.3, 10 lowest mode branches were calculated for 30 angles θ_1 in interval $0.589 < \theta_1 < 0.982$ (14 mode points at $\theta_1 = \pi/4$). The basis contained 100 eigenfunctions, $s_{max} = g_{max} = 10$. The branches 1, 2 ... 10 are highlighted by colour. The inclined arrows show angles of strengthened Bragg diffraction along the symmetry directions: 0.629, 0.657, 0.695 radians and three symmetrically reflected points with respect to the ΓM' direction ($\theta_1 = 0.785$). The calculated lowest energy is $\Omega_{min} \approx 0.006$ eV (branch 1) and the maximal energy 0.372 eV is reached by mode of branch 9 at $\theta_1 \approx 0.973$, whereas

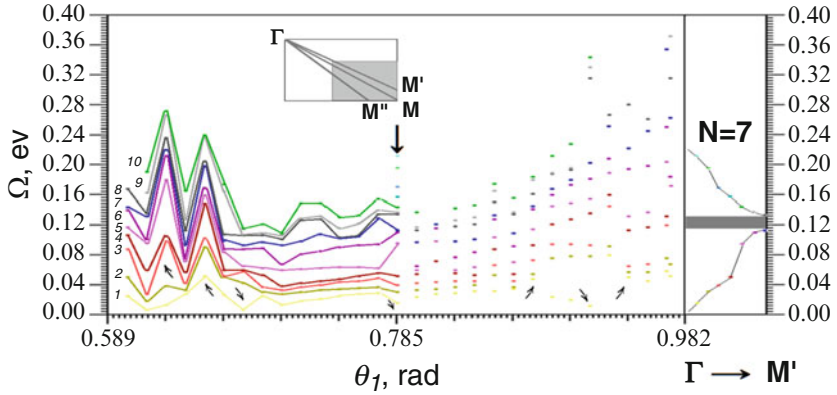

Fig. 18.3 Mode energy angular diagram of the 6 × 7-period (SiO_2/SiO_2) 2D IPCR. *Inset*: rectangular reciprocal lattice cell, symmetry directions: M', corresponds to $\theta_1 = \pi/4$; M, the resonator diagonal; M", elementary cell symmetry direction. *Mode energy diagram*. θ_1, plane wave incidence angle in the silicon glass matrix material within the TIR domain $0.589 < \theta_1 < 0.982$; 1,2...10, conventional lines (branches) uniting modal points at different θ_1 by increased number of nodal lines; $a_y = 1.5$ μm, $a_z = 1.0$ μm, well sizes $b_z = 1.0$ μm, $b_y = 2.0$ μm (bar material 4, Fig. 18.1); dielectric functions $\varepsilon_1 = 3.24$ (matrix); $\varepsilon_2 = 2.25$ (bar material 4); *inclined arrows* show angles of strengthened Bragg diffraction, *vertical arrow*, direction ΓM'. *Right panel*: generalized bandgap diagram for ΓM' direction ($N = 7$), first band, seven points, second band, seven points; gap is between 0.116 and 0.132 eV

in interval (0.922, 0.966) both branches 9 and 10 exceed the interval of calculation 0.4 eV. The calculations show that if N_z and N_y increase then all branches shift down and density of branches becomes larger. Therefore, the states existing in an infinite PhCr may be forbidden in a finite resonator.

In some sense the considered IPCR represents a generalization of a partial case of infinite PhCr when N_z, N_y should tend to infinity. The local density of modal points along energy axis increases with increasing N_z and N_y and simultaneously the all modal branches go down. Let us take into account that the number of eigenstates forming the band varies from 0 to N (number of periods in this direction) for the first band, from N to 2N for the second and so on. Therefore, to transfer from the modal branches representation to the conventional description of the bandgap structure we should step by step select N points

$$N = Int\left(\sqrt{N_z^2 \cos^2\theta_1 + N_y^2 \sin^2\theta_1}\right) \tag{18.8}$$

corresponding to the chosen angle θ_1. For the ΓM' direction ($\theta_1 = \pi/4$) the lowest *p*-polarized band of the generalized bandgap diagram is shown at the right side of Fig. 18.2. As far as the number of states in this direction $N = 7$, the first band consists of seven points projected from the ΓM' column of mode points (vertical arrow) to right in order of the mode energy and wave vector growth.

In a conventional case of an infinite photonic crystal, when the number of periods along the chosen direction ΓM' goes to infinity the number of points forming the curve also goes to infinity. The second band contains the next 7 modes numbered from 8 to 14 with energy growth. A partial gap arises between 0.116 and 0.132 eV. In the case of an infinite resonator, the modes became allocated along the band line everywhere densely though the point's density is expressed by the same formula "crystal size/2π". Here, we are considering *p*-polarized modes of the resonator. The linearly independent set of *s*-polarized modes form their own structure of branches and an additional band line arises in the ΓM' direction for each band.

If the resonator has the shape of a square and elementary cells are also squares, the calculated branches became allocated symmetrically as to the bisector $\theta_1 = \pi/4$. Besides, due to symmetry the modal branches are doubly degenerated. The decrease of symmetry leads to splitting of branches like what we can see for the considered IPCR. The SWE approach gives a smooth transformation of the considered IPCR (Fig. 18.1) to a structure with extremely increased d_y when the system becomes indistinguishable from a layered structure. Since the angular discreetness of spectrum arises due to the finite size of the resonator, we have got N angular-dependent mode branches inside every band of states [1, 9, 10].

18.4 Mode Energy Distribution Throughout the Island Resonator

The classification of the trapped inside the resonator modes is ruled by the Courant nodal line theorem [12, 13] claiming that for the system defined in the space R^m, the nodal set of eigenfunctions (modes) of Eq. (18.1) are locally composed of hypersurfaces of dimensions $m-1$. In particular, we have for $m = 2$ a set of nodal lines which are either closed or having their ends at the definitional domain. Due to the principally unlimited definitional domain of the problem under consideration, the nodal lines must be also nonrestricted. Several topology features should be noted for the modes of a 2D island kind resonator.

- The node lines of a mode reflects symmetry of the system and are divided into two types: longitudinally (along Z axis) and transversely oriented.
- The node lines of both types are infinite.
- The energy hierarchy of modes correlates with number of node lines within a given type.
- If one of two modes has one node line more, it has higher energy, ceteris paribus.

The latter statement is the consequence of the easy proven theorem: between the two nodal lines of a mode one can find a node line of the older mode with higher energy. The Courant nodal line theorem gives a base to test the results of calculation both the set of mode branches (eigenvalues) and mode coordinate dependencies (eigenfunctions). In general, the structure of island resonator modes

shows the expected similarity to that existing for transverse electromagnetic waves in rectangular and cylindrical waveguides [14, 15]. In Fig. 18.4a, the classification of lowest eigenstates in the IPCR is presented. Two factors influence the classification: number of node lines and correlation between them. The first circumstance leads to the shell structure of states when a shell unites modes with the same number of node lines. It is obvious that two types of node lines produce three kinds of modes: with node lines along Z axis, along Y axis and containing both transverse and longitudinal node lines. In Fig. 18.4a, the ground state is represented by a mode without nodal lines, first shell consists of two modes with one node line, second shell contains three two-node line states and so on. In accordance with the Courant theorem, every added node line, even of another type, increases energy of state. Nevertheless in a binary structure with rectangular (non-square) lattice, the modes containing node lines of one kind may form more or less densely the ladder of energy levels. In particular, if period $d_y > d_z$ then modes with transverse node lines have softer spectrum. Mixed modes occupy intermediate position. Therefore the shells have a tilt that makes energy hierarchy of states more complicate like it is shown in Fig. 18.3a. The discussed above smooth transformation of the IPCR to a structure with extremely large magnitudes d_y will express here in an essential reconstruction of modal structure: the left column remains the same, soft modes containing transverse node lines become practically indistinguishable from the left column modes with the same number of longitudinal nodal lines and vanish. As the result, the 2D energy angular diagram coincides with the spectrum angular diagram of a layered photonic crystal. The mode amplitudes $h^{\sigma}{}_{m}$ have a sense of a mode expansion coefficients in the $|s, g>$ basis. Following (18.5) and (18.6), we calculated the complete eigenvalue problem including both energies and eigenfunctions in basis $s_{\max} = g_{\max} = 10$. In Fig. 18.4b, spatial distribution for the lowest *6* modes $\sigma = 1,2...6$ at $\theta_1 = 0.785$ is shown. The calculated energies of states Ω_σ are *0.0116* eV, *0.031* eV, *0.040* eV, *0.052* eV, *0.096* eV and *0.112* eV. Though the nodal lines allocate in accordance with the Courant theorem (arrows), small deviations of symmetry in the distribution of modal amplitudes arise due to not too high accuracy of calculations (*0.01*).

To know the distribution of field density in the IPCR may be of importance in two aspects. First, pumping of a separate mode inside the resonator's TIR domain leads to accumulation of energy distributed throughout the IPCR. Therefore the output beam may be made of much more intensity than the input one. One more circumstance concerns an opportunity to use the distributed active impurities matching to a chosen mode.

18.5 Summary

Here the theory of a binary island kind photonic crystal resonator has been developed in the framework of standing wave expansion method. The 2D basis formation procedure was implemented with the use of analytically obtained two

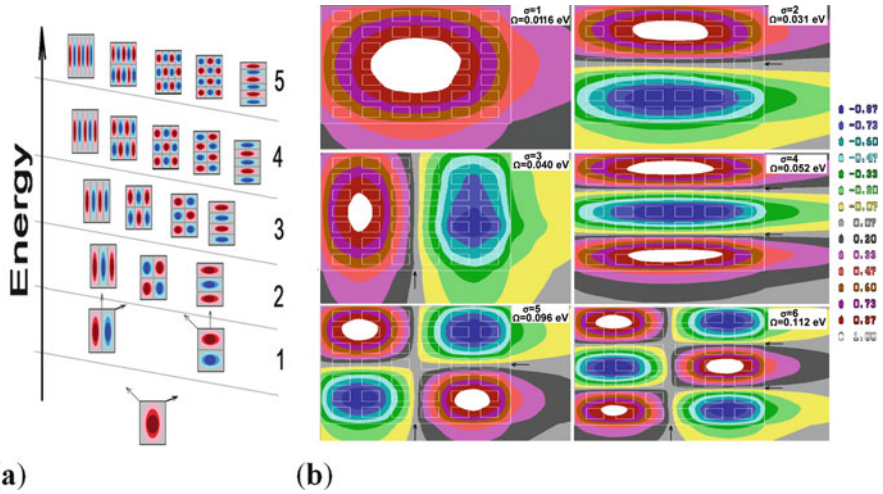

Fig. 18.4 (**a**) The eigenstates classification in an island kind 2D photonic crystal resonator, lowest 20 modes. Two systems of nodal lines, oriented along Z and Y axis; it is taken that Y direction has softer spectrum, 1, 2 . . . 5 shells of states; (**b**) Calculated field amplitude distribution for 6 lowest p-polarized modes $\sigma = 1..6$, of the 6×7-period (SiO_2/SiO_2) 2D IPCR (parameters are described in Fig. 18.3), ICPR mask, white lines, $\theta_1 = \pi/4$

1D basis sets for the two probe 1D structures and Courant's nodal line theorem in the process of basis generation. Electromagnetic energy distribution for some typical band, surface and edge modes of a 19×19 period photonic resonator were calculated. The procedure of the transfer to conventional band structure description was considered for a 6×7 period finite structure was investigated analytically and numerically. The classification concept of island kind resonator's modes is proposed. It worth noting that though the rectangular lattice was considered, the proposed SWE method for finite resonators may be adapted for any symmetry of the lattice as well as for any shape of bars in matrix.

References

1. Glushko EY, Glushko OE, Karachevtseva LA (2012) Photonic Eigenmodes in a photonic crystal membrane. ISRN Optics 2012:Article ID 373968:6p. doi:10.5402/2012/373968
2. Yablonovich E (1987) Inhibited spontaneous emission in solid state physics and electronics. Phys Rev Let 58:2059
3. John S, Joannopoulos D, Johnson SG, Winn JN, Meade RD (2008) Photonic crystals: molding the flow of light, 2nd edn. Princeton University Press, Princeton
4. Sakoda K (2001) Optical properties of photonic crystals. Springer, Berlin
5. Winn NY, Fink S, Fan Y, Joannopoulos JD (1998) Omnidirectional reflection from a one-dimensional photonic crystal. Opt Lett 23:1573–1575

6. Deopura M, Ullal CK, Temelkuran B, Fink Y (2001) Dielectric omnidirectional visible reflector. Opt Lett 26:1197–1199
7. Loncar M, Doll T, Vuchkovich J, Scherer A (2000) Design and fabrication of silicon photonic crystal optical waveguides. J Lightwave Technol 18:1402–1411
8. Jamois C, Wehrspohn RB, Andreani LC, Hermann C, Hess O, Gosele U (2003) Silicon-based two-dimensional photonic crystal waveguides. Photonics Nanostruct Fundam Appl 1:1–13
9. Glushko EY, Glushko AE, Karachevtseva LA (2010) Photonic membranes and photonic crystal resonators for all-optical signal processing. Proc SPIE 7713:77131D
10. Glushko EY (2014) Influence of oxidation on the spectrum of a ternary comb-like silicon photonic crystal: intrinsic modes, reflection windows and intrinsic contrastivity. Eur Phys J D 68:264
11. Glushko EY, Glushko AE, Evteev VN, Stepanyuk AN (2008) Electromagnetic eigenwaves in metastructures: perturbation theory method. Proc. SPIE. 6888:69880J–69880J-11
12. Courant R, Hilbert D (1953) Methods of mathematical Physics, vol 1. Interscience, New York
13. Gladwell GML, Zhu H (2002) Courant's nodal line theorem and its discrete counterparts. Q J Mech Appl Math 55(1):1–15
14. Orfanidis SJ Electromagnetic waves and antennas, Chapter 9. Online book: http://eceweb1.rutgers.edu/~orfanidi/ewa/ch09.pdf
15. Oron R, Davidson N, Friesem AA (2001) Transverse mode shaping and selection in laser resonators. In: Wolf E (ed) Progress in optics 42. Elsevier Science, Burlington